Journal of the Mechanics and Physics of Solids 59 (2011) 775–786

Contents lists available at ScienceDirect

Journal of the Mechanics and Physics of Solids

journal homepage: www.elsevier.com/locate/jmps?

A comparative study of fracture in Al: Quantum mechanical vs. empirical atomistic description

Qing Peng [1], Gang Lu *

Department of Physics and Astronomy, California State University Northridge, Northridge, CA, USA

ARTICLE INFO

Article history:
Received 18 July 2009
Received in revised form
4 October 2010
Accepted 16 January 2011
Available online 25 January 2011

Keywords:
Plastic deformation
Dislocations
First-principles electron structure theory
Atomistic simulation
Fracture mechanics

ABSTRACT

A comparative study of fracture in Al is carried out by using quantum mechanical and empirical atomistic description of atomic interaction at crack tip. The former is accomplished with the density functional theory (DFT) based quasicontinuum method (QCDFT) and the latter with the original quasicontinuum method (EAM-QC). Aside from quantitative differences, the two descriptions also yield qualitatively distinctive fracture behavior. While EAM-QC predicts a straight crack front and a micro-twinning at the crack tip, QCDFT finds a more rounded crack profile and the absence of twinning. Although many dislocations are emitted from the crack tip in EAM-QC, they all glide on a single slip plane. In contrast, only two dislocations are nucleated under the maximum load applied in QCDFT, and they glide on two adjacent slip planes. The electron charge density develops "sharp corners" at the crack tip in EAM-QC, while it is smoother in QCDFT. The physics underlying these differences is discussed.

1. Introduction

Understanding fracture behavior in materials is a challenging undertaking. Despite nearly a century of study, several important issues remain unresolved. For example, there is little fundamental understanding of brittle-to-ductile transition as a function of temperature in many materials; there is still no definitive explanation of how fracture stress is transmitted through plastic zones at crack tips; and there is no complete understanding of the disagreement between theory and experiment regarding the limiting speed of crack propagation. These difficulties to a great extent stem from the fact that fracture phenomena are governed by processes occurring over a wide range of length and time scales; these processes are all connected and all contribute to the total fracture energy (Van der Giessen and Needleman, 2002).

As emphasized by Van de Giessen and Needleman, although the atomistic interaction at a crack tip may only account for a small fraction of the total fracture energy, it can be a controlling factor—after all, all fractures take place by breaking atomic bonds. Critical atomistic information, such as surface energy, stacking fault energy, dislocation nucleation/propagation energy and twinning formation energy, etc., has been known to play central roles in fracture. In fact, some of these quantities are at the heart of fracture mechanics, including Griffith's (1920) criterion for brittle fracture, Rice's (1992) criterion for crack tip blunting and more recently a criterion for twinning at crack tips (Tadmor and Hai, 2003), to name a few.

Because of the inherent multiscale nature of fracture—the process at each scale depends strongly on what happens at the other scales, the modeling and simulation of fracture calls for *concurrent* multiscale approaches (Lu and Kaxiras, 2005). One of the first concurrent multiscale modeling of fracture was based on macroscopic atomistic *ab initio* dynamics (MAAD)

* Corresponding author. Tel.: +1 818 677 2021.
E-mail addresses: qpeng.org@gmail.com (Q. Peng), ganglu@csun.edu (G. Lu).
[1] Tel.: +1 818 671 7005.

0022-5096/$ - see front matter © 2011 Elsevier Ltd. All rights reserved.
doi:10.1016/j.jmps.2011.01.008

method for silicon (Broughton et al., 1999). MAAD couples a quantum mechanical description of atoms at a crack tip, to an empirical (or classical) atomistic description of atoms at a short distance away from the crack tip, and to the continuum finite-element description of the rest of the system. Since MAAD, several other concurrent multiscale methods have been developed, all involving some level of quantum mechanical modeling at the crack tip (Csányi et al., 2004; Bernstein and Hess, 2003; Ogata et al., 2001). All these methods were developed/applied for Si owning to the following technical reasons: (1) large-scale electronic structure methods such as linear-scaling algorithms are only applicable to covalently bonded semiconductors like Si; general approaches for metals are still under development; (2) satisfactory QM/MM coupling schemes for metals were less well developed until recently (Bernstein et al., 2009; Liu et al., 2007; Zhang and Lu, 2007). However, concurrent multiscale approaches that do not involve quantum mechanics are readily available (Miller et al., 1998; Kohlhoff et al., 1991; Buehler et al., 2006). Among them, quasicontinuum (QC) method is particularly promising and it has been widely applied to many material problems, including fracture in metals (Tadmor and Miller, 2005). QC strives to achieve a "seamless" coupling between atomistic and continuum descriptions and allows quantum mechanical interactions incorporated in a systematical manner. For example, although the original QC was based on classical atomic interactions, significant progress has been made recently to incorporate quantum mechanical interactions in the local QC region (Hayes et al., 2006), nonlocal QC region (Lu et al., 2006) and entire QC system (Peng et al., 2008). The coarse-graining strategy of QC has also been explored to perform large-scale electronic structure calculations (Gavini et al., 2007).

Despite the impressive advance in multiscale methodology development, a crucial aspect of fracture modeling has not been addressed. Although it is clear that an atomistic description at crack tips is indispensable for many purposes, it is not well established whether a quantum mechanical description at the crack tips is truly necessary. This is a poignant point given the continuing improvement of empirical potentials and the still heavy costs of quantum simulations. It is to address this question that motivates the present study. As a first look at the problem, we focus on crack tip plasticity in Al and compare results received from a quantum mechanical description vs. an empirical atomistic description at the crack tip, both in the framework of QC. Since the atomistic resolution is only necessary near the crack tip while the linear elastic fracture mechanics boundary conditions can be applied to the far field, QC is well poised for such fracture simulations. In addition, QC simulations involve quasi-static energy minimization, thus the unrealistically high strain rates common to molecular dynamics simulations are avoided. Unfortunately, as a result thermally activated processes are precluded in QC. Al is chosen in this study because it is relatively inexpensive for the density functional theory (DFT) calculations and an excellent embedded-atom-method (EAM) empirical potential exists for Al (Ercolessi and Adams, 1994). The goal of this work is to examine how and why the results of the empirical simulations differ from those of quantum mechanical DFT simulations at the crack tip. To this end, we employ the so-called QCDFT method in which the nonlocal atoms at the crack tip are treated with DFT. The QCDFT results are compared to those obtained from the original QC method in which all nonlocal atoms are treated with EAM empirical potential.

The structure of the paper is as follows. The methodology is introduced in Section 2 for both QC and QCDFT methods. A semi-infinite crack under mode I loading is set up in Section 3.1. The computational parameters are described in Section 3.2 and the loading procedure for the crack is summarized in Section 3.3. The simulation results and analysis are presented in Section 4 and discussions are given in Section 5. Finally we conclude in Section 6.

2. Methodology

The QC method (Shenoy et al., 1999; Tadmor et al., 1999) is a multiscale approach (Lu and Kaxiras, 2005) that combines atomistic models with continuum theories, and thus offers an advantage over conventional atomistic simulations in terms of computational efficiency. The idea underlying the QC method is that atomistic processes of interest often occur in very small spatial domains (e.g., crack tip) while the vast majority of atoms in the material behave according to well-established continuum theories. To exploit this fact, the QC method retains atomic resolution only where necessary and coarsens to a continuum finite-element description elsewhere. This is achieved by replacing the full set of N atoms with a small subset of N_r "representative atoms" or *repatoms* ($N_r \ll N$) that approximate the total energy through appropriate weighting. The energies of individual repatoms are computed in two different ways depending on the deformation in their immediate vicinity. Atoms experiencing large deformation gradients on an atomic-scale are computed in the same way as in a standard fully atomistic method. In QC these atoms are called *nonlocal* atoms. In contrast, the energies of atoms experiencing a smooth deformation field on the atomic scale are computed based on the deformation gradient in their vicinity as befitting a continuum model. These atoms are called *local* atoms. The total energy E_{tot} (which for a classical system can be written as $E_{\text{tot}} = \sum_{i=1}^{N} E_i$, with E_i the energy of atom i) is approximated as

$$E_{\text{tot}}^{\text{QC}} = \sum_{i=1}^{N^{\text{nl}}} E_i(\{\mathbf{q}\}) + \sum_{j=1}^{N^{\text{loc}}} n_j E_j^{\text{loc}}(\{\mathbf{F}\}). \tag{1}$$

The total energy has been divided into two parts: an atomistic region of N^{nl} nonlocal atoms and a continuum region of N^{loc} local atoms ($N^{\text{nl}} + N^{\text{loc}} = N^r$).

The original formulation of QC was limited to classical potentials for describing interactions between atoms. However, since many material properties depend crucially on the behavior of electrons, such as bond breaking/forming at crack tips or defect cores, chemical reactions with impurities, surface reactions and reconstructions, electron excitation and magnetism,

etc., it is desirable to incorporate appropriate quantum mechanical descriptions into the QC formalism. QCDFT is one strategy to fill this role. In specific, QCDFT combines the coarse graining idea of QC and the coupling strategy of quantum mechanics/molecular mechanics (QM/MM) approaches. Therefore QCDFT can capture the electronic structure at the crack tip within the accuracy of DFT and at the same time reach the length-scale that is relevant to experiments (Lu et al., 2006; Peng et al., 2008).

The original QC formulation assumes that the total energy can be written as a sum over individual atom energies. This condition is not satisfied by quantum mechanical models. To address this limitation, in the present QCDFT approach the nonlocal region is treated by an EAM-based QM/MM coupling approach (Lu et al., 2006; Liu et al., 2007): the Kohn–Sham density functional theory (KS-DFT) is coupled to EAM with the interaction energy calculated also by EAM. The local region, on the other hand, is dealt with by EAM, which is the same energy formulation used in the MM part of the nonlocal region. This makes the passage from the atomistic to continuum seamless since the same underlying material description is used in both. This description enables the model to adapt automatically to changing circumstances (e.g. the nucleation of new defects or the migration of existing defects). The adaptability is one of its main strengths of QC and QCDFT, which is missing in many other multiscale methods.

More specifically, in the present QCDFT approach the material of interest is partitioned into three distinct domains: (1) a nonlocal quantum mechanical DFT region (region I); (2) a nonlocal classical region where classical EAM potentials are used (region II); and (3) a local region (region III) that employs the same EAM potentials as region II. The coupling between regions II and III is achieved via the QC formulation, while the coupling between regions I and II is accomplished by the QM/MM scheme (Choly et al., 2005; Liu et al., 2007). The total energy of the QCDFT system is then given by (Lu et al., 2006)

$$E_{\mathrm{tot}}^{\mathrm{QCDFT}} = E^{\mathrm{nl}}[\mathrm{I}+\mathrm{II}] + \sum_{j=1}^{N^{\mathrm{loc}}} n_j E_j^{\mathrm{loc}}(\{\mathbf{F}\}) = E_{\mathrm{DFT}}[\mathrm{I}] - E_{\mathrm{EAM}}[\mathrm{I}] + E_{\mathrm{EAM}}[\mathrm{I}+\mathrm{II}] + \sum_{j=1}^{N^{\mathrm{loc}}} n_j E_j^{\mathrm{loc}}(\{\mathbf{F}\}), \tag{2}$$

where $E^{\mathrm{nl}}[\mathrm{I}+\mathrm{II}]$ is the total energy of the nonlocal region (I and II combined with the assumption that region I is embedded within region II), $E_{\mathrm{DFT}}[\mathrm{I}]$ is the energy of region I in the absence of region II computed with DFT, $E_{\mathrm{EAM}}[\mathrm{II}]$ is the energy of region II in the absence of region I computed with EAM, and $E_{\mathrm{EAM}}[\mathrm{I}+\mathrm{II}]$ is the energy of the nonlocal region computed with EAM.

Other types of combination with quantum mechanical and classical atomistic methods may also be implemented in QCDFT. The great advantage of the present implementation is its simplicity; it demands nothing beyond what is required for a DFT calculation and an EAM-QC calculation. Another important practical advantage of QCDFT method is that, if region I contains many different atomic species while region II contains only one atom type, there is no need to develop reliable EAM potentials that can describe each species and their interactions. This is because if the various species of atoms are well within region I, the energy contributions of these atoms are canceled out in the total energy calculation. This advantage renders the method particularly useful in dealing with impurities, which is an exceedingly difficult task for empirical potential simulations.

The equilibrium structure of the system is obtained by minimizing the total energy in Eq. (2) with respect to all degrees of freedom. Because the time required to evaluate $E_{\mathrm{DFT}}[\mathrm{I}]$ is considerably more than that required for computation of the other EAM terms in $E_{\mathrm{tot}}^{\mathrm{QCDFT}}$, an alternate relaxation scheme turns out to be useful. The total system can be relaxed by using conjugate gradient approach on the DFT atoms alone, while fully relaxing the EAM atoms in region II and the displacement field in region III at each step. An auxiliary energy function can be defined as

$$E'[\{\mathbf{q}^{\mathrm{I}}\}] \equiv \min_{\{\mathbf{q}^{\mathrm{II}}\},\{\mathbf{q}^{\mathrm{III}}\}} E_{\mathrm{tot}}^{\mathrm{QCDFT}}[\{\mathbf{q}\}], \tag{3}$$

which allows for the following relaxation scheme: (i) minimize $E_{\mathrm{tot}}^{\mathrm{QCDFT}}$ with respect to the atoms in regions II ($\{\mathbf{q}^{\mathrm{II}}\}$) and the atoms in region III ($\{\mathbf{q}^{\mathrm{III}}\}$), while holding the atoms in region I fixed; (ii) calculate $E_{\mathrm{tot}}^{\mathrm{QCDFT}}[\{\mathbf{q}\}]$, and the forces on the region I atoms; (iii) perform one step of conjugate gradient minimization of E'; (iv) repeat until the system is relaxed. In this manner, the number of DFT calculations performed is greatly reduced, albeit at the expense of more EAM and local QC calculations. A number of tests have shown that the total number of DFT energy calculations for the relaxation of an entire system is about the same as that required for DFT relaxation of region I alone.

The QC partitioning of the physical system into two regions causes an unphysical mismatch between the energy functional evaluated in the local and nonlocal regions. As a result, spurious forces near the interface appear and they are called ghost forces in the QC literature (Shenoy et al., 1999; Tadmor et al., 1999). The nature of the ghost force has been well understood and robust schemes have been developed to reduce the ghost force (Shenoy et al., 1999; Tadmor et al., 1999). Similarly, coupling errors exist at the QM/MM interface, due to the different descriptions of QM and MM for the same surface at the QM/MM boundary. The coupling errors have been well studied and effective methods have been proposed to reduce the errors significantly (Liu et al., 2007).

3. Computational details

3.1. Model setup

A semi-infinite crack in a single Al crystal is studied by both QC and QCDFT for comparisons. The crack is made by removing two layers of atoms with $x<0$ and $y=0$ and 1.41 Å. The crack plane is $(\bar{1}\,1\,0)$ and in this orientation, $(1\,1\,1)$

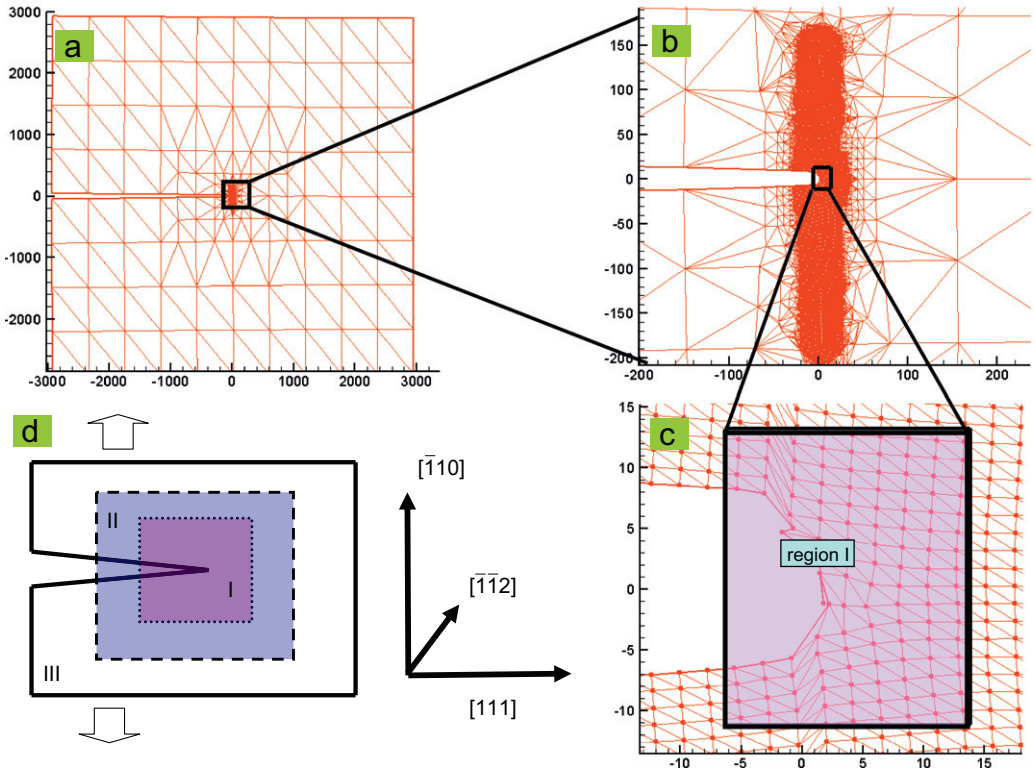

Fig. 1. (a) The overview of the entire crack system with finite-element mesh; (b) a blown-up view of (a) showing the nonlocal region; (c) region I box and atomic structure at the crack tip; (d) schematic partition of the system into regions I, II and III. The *x*, *y* and *z* axes is along [1 1 1], [$\bar{1}$ 1 0] and [$\bar{1}$ $\bar{1}$ 2] respectively. All lengths are in Å.

plane is the only active slip plane for dislocations emitted from the crack tip; all other {1 1 1}-type planes lie obliquely to the crack plane and are thus precluded by the imposed plane strain conditions (Tadmor and Hai, 2003). This configuration was used previously in a MD study by Hoagland et al. (1990) and an EAM-QC study by Hai and Tadmor (2003) although the initial crack opening and the EAM potential used are different in these studies. The initial crack opening in the present work is determined based on two competing considerations: (1) it cannot be too narrow otherwise the crack will close and/or large number of loading steps is required to observe the onset of plasticity; (2) it cannot be too wide otherwise the DFT region is too large to render calculations feasible. Of course, the DFT region has to be large enough to capture the crucial plasticity events at the crack tip. The crack is subject to mode I loading along *y* direction shown schematically in Fig. 1(d).

The dimensions of the system are $6000 \times 6000 \times 4.887$ Å^3 along the *x*, *y*, *z* directions respectively. The system is periodic in *z*-direction, and has Dirichlet boundary conditions in the other two directions. The system contains over 11 million Al atoms—a size that is well beyond the reach of any full-blown quantum calculation. The schematic overview of the system is shown in panel (a) of Fig. 1 with finite-element meshes. Panel (b) is a zoomed-in view of the nonlocal region and panel (c) displays the atomic detail of the crack tip.

3.2. Computational parameters

Two comparative calculations are carried out for the crack: EAM-QC vs. QCDFT for Al. EAM-QC is the original QC with EAM potential for atomic interactions. In this work, the EAM potential used is rescaled from the original "force-matching" EAM (Ercolessi and Adams, 1994) potential so that it matches precisely the value of the lattice constant and bulk modulus of Al from the DFT calculations (Choly et al., 2005). Although the re-scaling changes very little to the original potential, it eliminates lattice parameter mismatch at the QM/MM interface, and thus reduce QM/MM coupling errors.

DFT calculations are carried out with the Vienna *ab initio* simulation package (VASP) (Kresse and Hafner, 1993, 1994; Kresse and Furthuller, 1996a, b) which is based on Kohn–Sham density functional theory (KS-DFT) with the local density approximation and ultrasoft pseudo-potentials. A plane-wave cutoff of 129 eV is used in the calculations and the *k*-points are sampled according to the Monkhorst and Pack (1976) method with a $1 \times 1 \times 9$ mesh in the Brillouin zone. There are around 134 DFT atoms in region I.

3.3. Loading procedure

The simulations are performed quasi-statically with displacement boundary conditions where the displacement is prescribed as a function of intended stress intensity factor (SIF) at each loading step. For EAM-QC, the loading procedure is outlined as following:

(1) For a small initial stress intensity factor K_I, the anisotropic linear elastic fracture mechanics (LEFM) solution (Sih and Liebowitz, 1968) $\mathbf{u}_{LEFM}(\mathbf{X},K_I)$ is obtained. Each atom is displaced according to $\mathbf{u}(\mathbf{X})=\mathbf{u}_{LEFM}(\mathbf{X},K_I)$, where $\mathbf{u}$ is the displacement field and $\mathbf{X}$ is the position of nodes in the model.

(2) The displacement at the model boundaries is fixed except for the crack surfaces; the positions for all repatoms are obtained by energy minimization as explained before.

(3) The finite-element mesh, the status of repatoms (local vs. nonlocal) and the neighbor list are updated.

(4) The SIF is increased by a small amount ΔK_I as $K_I = K_I + \Delta K_I$ and repeat from step (1) until the intended SIF is achieved.

In this study the increment $\Delta K_I = 0.001$ eV/Å$^{2.5}$ is used. The loading procedure adopted here follows closely that of Hai and Tadmor (2003).

Because DFT calculations are much more expensive than EAM, we use EAM-QC to load the crack until an incipient plasticity is about to take place, at which point QCDFT is switched on. In other words, a QCDFT relaxation starts from a configuration that is obtained by EAM-QC for K_I. QCDFT then increases the SIF by ΔK_I. This is a reasonable approximation because EAM is known to give accurate results for deformations prior the onset of crack tip plasticity or the appearance of lattice defects. As will be shown later, since the critical load for the onset of plasticity from QCDFT is smaller than that from EAM-QC, the present loading strategy does not run the risk of missing incipient plasticity of QCDFT.

4. Results and analysis

4.1. EAM-QC calculation of Al

To establish the validity of present EAM-QC method, we first perform EAM-QC calculations for the same crack studied in Hai and Tadmor (2003). We use the same EAM potential and the same initial crack opening as that in the above reference. The results are presented in Fig. 2 where two edge dislocations are emitted from the crack tip and they glide at the same slip plane in a symmetrical manner. The critical SIF is 0.144 eV/Å$^{2.5}$. All these results are identical to those found in Hai et al. and thus validate the present EAM-QC method.

Next, we apply EAM-QC to the crack of interest. The crack is loaded quasi-statically and no crack tip plasticity is observed until the SIF reaches K_I =0.180 eV/Å$^{2.5}$. By comparison, the critical SIF for a pure brittle cleavage computed from the Griffith criterion for this orientation is K_{Ic}=0.205 eV/Å$^{2.5}$. In Fig. 3, we present the out-of-plane displacement U_z as a function of applied K_I values. For K_I =0.179 eV/Å$^{2.5}$, although no dislocation is observed, significant deformation at the crack tip is clearly visible (panel a). At K_I=0.180 eV/Å$^{2.5}$, the first dislocation is nucleated and subsequently moves away from the crack tip. The dissociated $1/2[1\ \bar{1}\ 0]$ edge dislocation is stabilized at about 70 Å below the crack on a (1 1 1) plane (panel b). The contour shading of Fig. 3 corresponds to the magnitude of U_z, whose nonzero values indicate that the edge

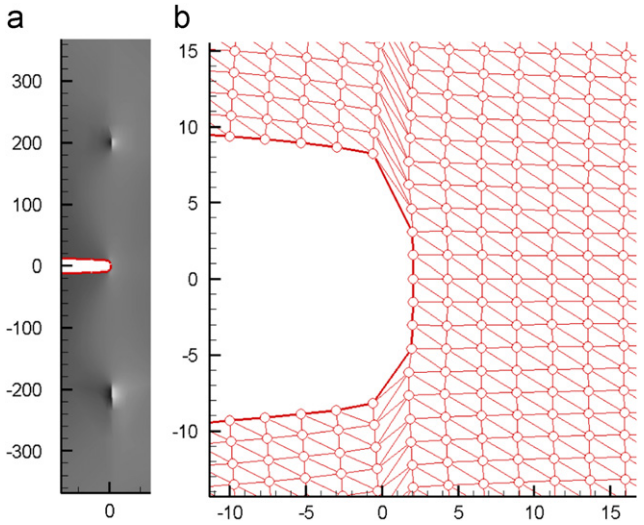

Fig. 2. EAM-QC results at SIF K_I=0.144 eV/Å$^{2.5}$. (a) The out-of-plane displacement U_z; the displacement contours range from −0.5 Å (darkest) to 0.5 Å (lightest). (b) The zoomed-in view of the crack tip atomic structure and finite-element mesh. The open circle represents the atomic position. All distances are in Å.

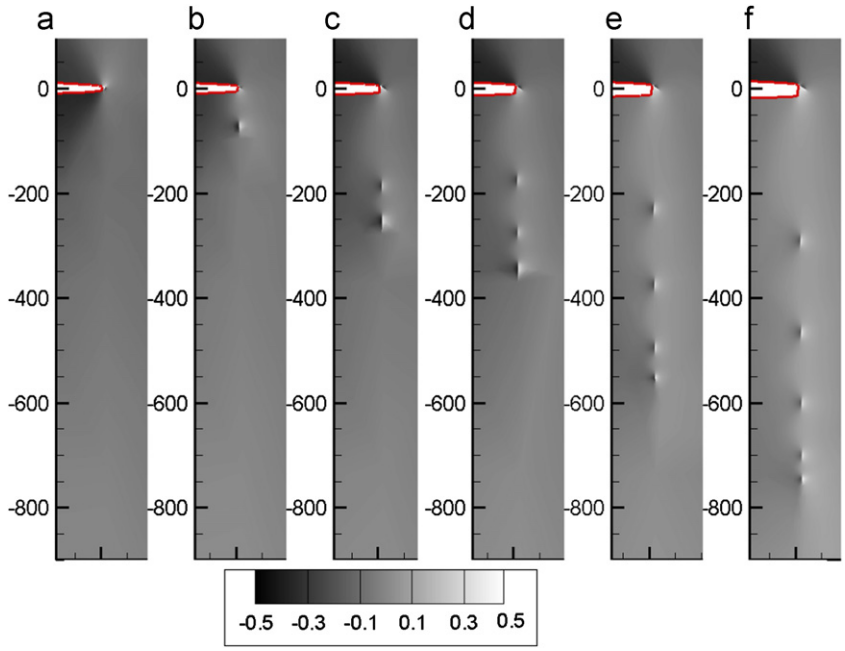

Fig. 3. The out-of-plane displacement U_z obtained from the EAM-QC calculations at SIF K_I of (a) 0.179, (b) 0.180, (c) 0.184, (d) 0.186, (e) 0.191, and (f) 0.198 eV/Å$^{2.5}$ respectively. The displacement contours range from -0.5 Å (darkest) to 0.5 Å (lightest). The crack surfaces are represented by red curves. All distances are in Å. (For interpretation of the references to color in this figure legend, the reader is referred to the web version of this article.)

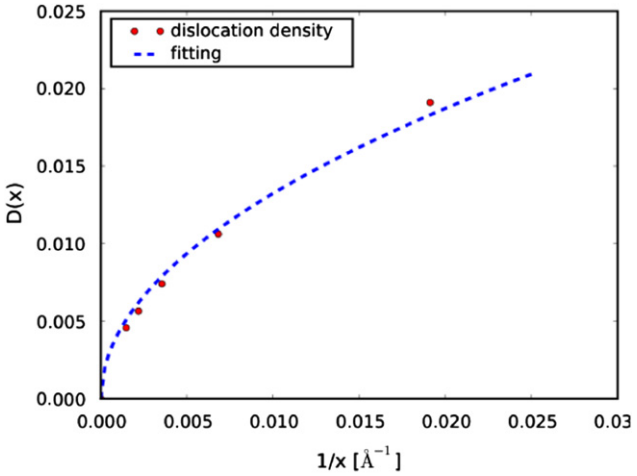

Fig. 4. The dislocation distribution function $D(x)$ as a function of the inverse of the distance x. The dashed curve is a fit to the filled circles.

dislocation is dissociated into partials. Interestingly, at the same time, a micro-twin is also nucleated from the crack tip (Fig. 5a). The micro-twin is two layers in both length and width, the twinning direction is [7 1 4] and the twinning plane is $(1\ \bar{3}\ \bar{1})$. As K_I value is increased, more dislocations are emitted on the (1 1 1) plane and *at the same time*, the micro-twin grows in length but not in width. More specifically, as K_I increases to 0.184, 0.186, 0.191, 0.198 eV/Å$^{2.5}$, two, three, four and five dislocations are emitted from the crack tip and they glide on the same (1 1 1) plane, as shown in the panel of (c), (d), (e) and (f) of Fig. 3 respectively. Correspondingly, the micro-twin grows to three, four, five and six layers in length respectively. The micro-twin structures of two, three, five and six layers in length are shown in the panel of (a), (b), (c), (d) of Fig. 5 respectively. The width of the micro-twin is not increasing perhaps due to unfavorable stacking fault energy along the usual twinning plane. The reasonthat the twinning was not observed in Hai et al. is probably due to the different initial crack openings rather than the different EAM potentials used. We have done additional calculations for the present crack opening (2 layers) with the same EAM potential used in Hai and Tadmor (2003) and found a similar twinning at the crack tip. The emitted dislocations share the following characteristics: (1) they are all edge dislocations of $1/2[1\ \bar{1}\ 0]$ Burgers vector and dissociated into Shockley partials with a separation distance of 16 Å. This result agrees with the previous study

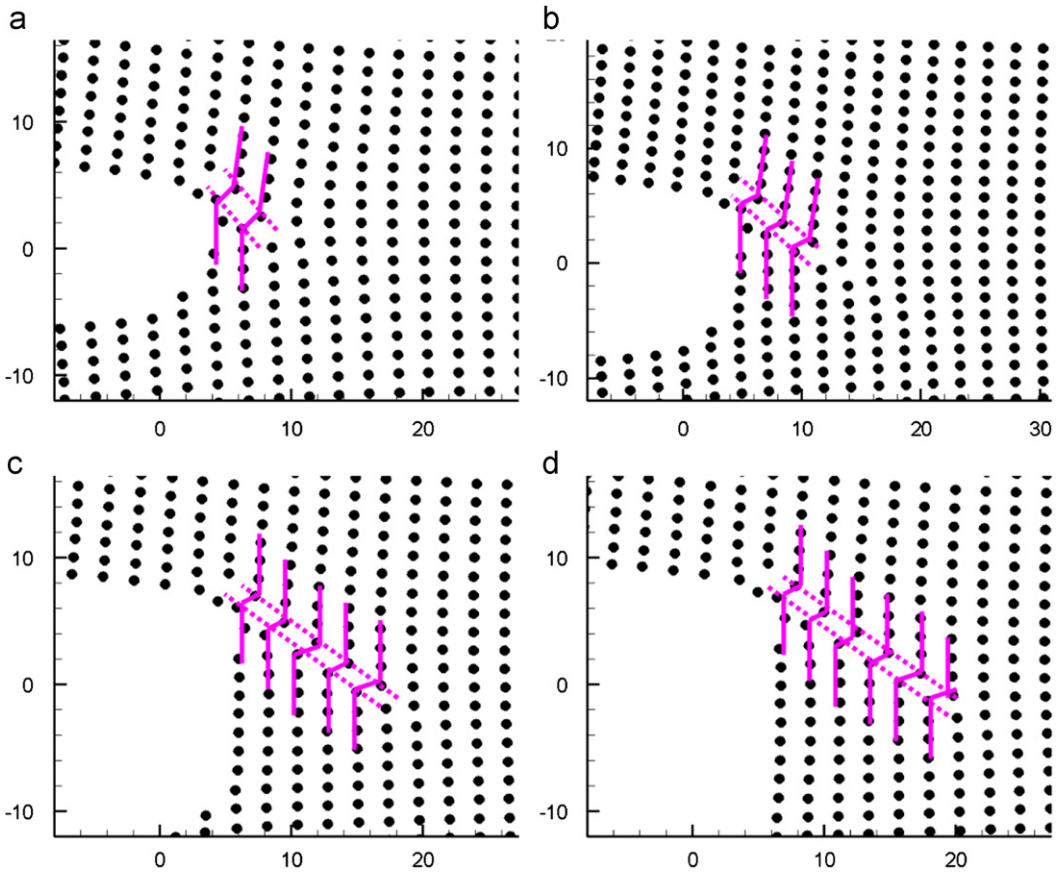

Fig. 5. Atomic structure at the crack tip from EAM-QC. Some of the atomic planes are highlighted in pink to indicate the twin. Dashed lines represent the two-layer twin. (a) K_I=0.180, (b) K_I=0.184, (c) K_I=0.191, (d) K_I=0.198 eV/Å$^{2.5}$. All distances are in Å. (For interpretation of the references to color in this figure legend, the reader is referred to the web version of this article.)

of Hai et al. with the similar EAM potential. But this value is too large compared to the experimental splitting distance of 5.5 Å, measured by Mills and Stadelmann (1989). The discrepancy may be attributed to still too low stacking fault energy of the EAM potential. (2) They are all on the same {1 1 1} slip plane whose position is $x=a/2$, where is a is (1 1 1) interplane distance. The active slip plane is slightly ahead of the crack front position at $x=0$. The emitted dislocations move away from the crack tip and form a pileup against the local/nonlocal QC interface. For K_I=0.198 eV/Å$^{2.5}$, the dislocation density $D(x)$ defined as the number of dislocations per unit distance along pileup line is found to be the square root of the inverse of the distance (Hirth and Lothe, 1970). The distance x refers to the distance between the dislocation center and the local/nonlocal interface. The fitted curve (dashed line) in Fig. 4 qualitatively agrees well with the elastic theory where the fitting function is given as $D(x)=0.13236\ (1/x)^{1/2}$.

4.2. QCDFT calculation of Al

The crack is first loaded by EAM-QC until K_I reaches 0.169 eV/Å$^{2.5}$ at which point QCDFT is switched on. This critical loading is determined by trial and error; we launch a number of QCDFT calculations at different K_I from previously relaxed EAM-QC structures and examine whether any crack tip plasticity is taking place. The smallest K_I value that results in incipient plasticity is the critical loading, 0.169 eV/Å$^{2.5}$. In comparison, the critical SIF for a pure brittle cleavage computed from the Griffith criterion is K_{Ic}=0.267 eV/Å$^{2.5}$.

The crack tip behavior of QCDFT is quite different from that of EAM-QC. At K_I=0.169 eV/Å$^{2.5}$, two dissociated edge dislocations are nucleated—one above the crack plane and one below it. In contrast to EAM-QC, the two dislocations glide at two *adjacent* (1 1 1) slip planes, as shown in Fig. 7(d). The positions of the two slip planes are at $x=-a/2$ and $x=-3a/2$ respectively; they are slightly behind the crack front position. The separation distance of the two Shockley partials is 16 Å, the same as that in EAM-QC calculation. This result is consistent with the fact that the dislocation cores are outside the DFT box where atomic interaction is determined by the rescaled EAM potential.

As the load is increased, the two emitted dislocations are driven further away from the crack plane, however, no more dislocation is nucleated within the maximum load that we have explored in this study. For the largest K_I=0.178 eV/Å$^{2.5}$,

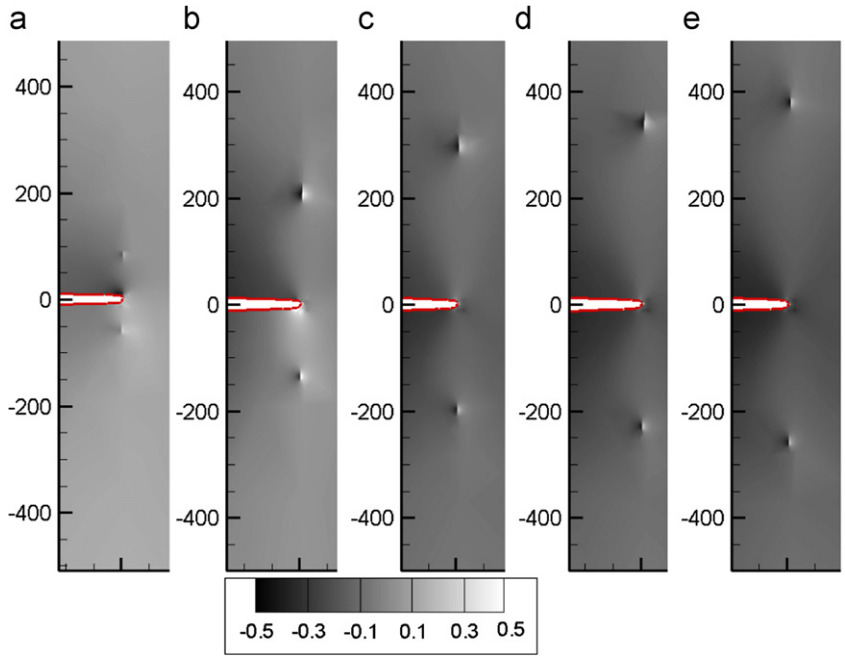

Fig. 6. The out-of-plane displacement U_z obtained from QCDFT calculations at SIF K_I of (a) 0.169, (b) 0.170, (c) 0.174, (d) 0.175 (e) 0.178 eV/Å$^{2.5}$ respectively. The displacement contours range from −0.5 Å (darkest) to 0.5 Å (lightest). All distances are in Å. (For interpretation of the references to color in this figure legend, the reader is referred to the web version of this article.)

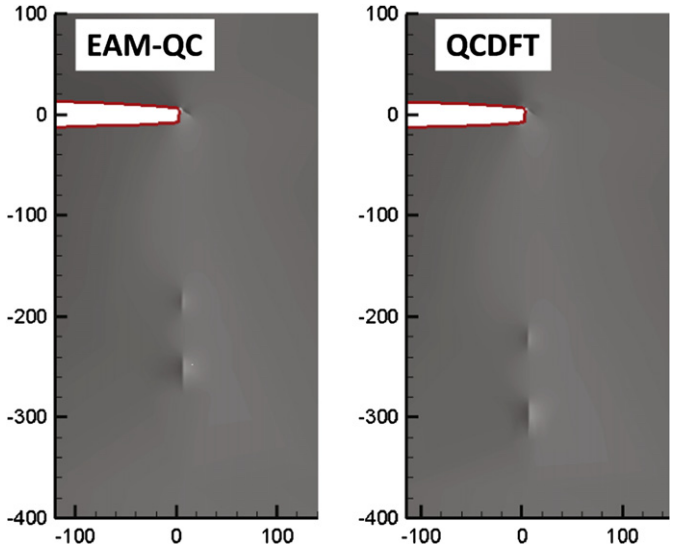

Fig. 7. The out-of-plane displacement U_z obtained from EAM-QC (left) and QCDFT (right) calculations at SIF K_I of 0.184 eV/Å$^{2.5}$. The displacement contours range from −0.5 Å (darkest) to 0.5 Å (lightest). All distances are in Å.

there are only two emitted dislocations gliding at 380 Å (up) and 258 Å (down) away from the crack plane. We have also increased the size of the DFT region, from 134 DFT atoms to 190 DFT atoms, but found that the results remain the same—the two emitted dislocations are located at 380 Å (up) and 260 Å (down) away from the crack plane. Although the computational effort of 190 atoms approaches the upper bound of DFT calculations, there is no guarantee that the results are fully converged—although there is a good indication that it is the case. Therefore, we should remain cautious that these results are considered correct only in the context of the present simulation capability.

To examine whether the number of nucleated dislocations in QCDFT has to do with the fact that there are two slip planes involved in QCDFT, we have carried out the following calculation. The EAM-QC calculation is first performed with

the loading K_I=0.184 eV/Å$^{2.5}$ and two dislocations are emitted at the same slip plane below the crack tip, shown in Fig. 7. Subsequently, the QCDFT is turned on with the EAM-QC result as the initial structure. And we find that the number of emitted dislocations remains two and both of them are located at the same slip plane. However, the dislocations in QCDFT move further away from the crack tip; they are stabilized at -222 and -298 Å respectively below the crack tip, comparing to -185 and -253 Å respectively in EAM-QC. Therefore, the number of nucleated dislocations observed in QCDFT is not the direct consequence of the two active slip planes.

Due to the computational cost of QCDFT, we did not pursue more calculations for even larger loadings. However, it is evident from the present study that the crack tip plasticity observed in QCDFT is *qualitatively different* from that in EAM-QC. The differences are striking given the fact that the QCDFT results are obtained following the relaxed EAM-QC configurations at smaller loadings.

5. Discussion

5.1. Dislocation nucleation at the crack tip

EAM-QC shows that the crack blunts by emitting dislocations gliding on a single slip plane, and the number of emitted dislocations increases as the SIF is increased. However, QCDFT predicts that two dislocations are nucleated from the crack tip and they glide at two adjacent slip planes. Moreover, the number of emitted dislocations remains the same (two) for all SIFs. These distinctions are highlighted in Fig. 8 where schematic diagrams, displacement contours and atomic structures at the crack tip for the two calculations are presented. In the schematic diagrams (a and d), the crack tip is represented by solid black lines/curves, and the dotted black lines denote the three relevant (1 1 1) slip planes at $x=-3/2a$, $-a/2$ and $a/2$. The stacking fault between the Shockley partials is indicated by a short red line segment. The displacement contour plots are the same as those shown in Figs. 3 and 6; they are reproduced here for convenience to the reader. The open circles in the atomic structure plots represent atomic positions. The sheared finite-element mesh in the atomic structure plots is the result of passing-by dislocations (the amount of shear corresponds to the net Burgers vector of the dislocations). The crack tip profile is approximated by blue line segments in the atomic structure plots. In Fig. 8(c) the crack tip profile is approximated by rectangular line segments $\overline{AB}+\overline{BD}+\overline{DE}$ to model the fact that the crack tip is blunted by emitting dislocations on a single slip plane. The active slip plane is represented by $\overline{BD}$ whose position is at $x = a/2$. In Fig. 8(f), however, the crack tip profile of QCDFT is approximated by zigzag line segments $\overline{AC}+\overline{CE}$ because two adjacent slip planes are activated, and their positions are at $x=-a/2$ and $x=-3/2a$.

To understand the origin of the differences, we resort to a simple model that captures the essential features of the crack configuration shown in Fig. 9. One can consult Fig. 8 to understand the correspondence between the model and the actual crack tip configuration. The reason why the rectangular segments $\overline{AB}+\overline{BD}+\overline{DE}$ are preferred in EAM-QC while the zigzag

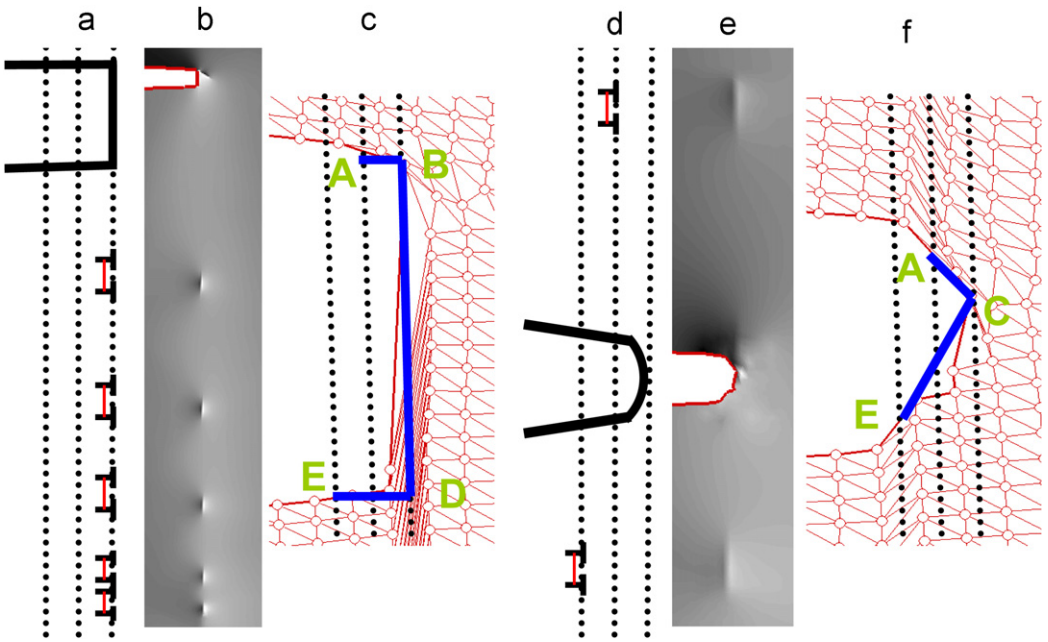

Fig. 8. The schematic diagram, displacement contours and atomic structure with finite-element mesh showing the dislocation pattern at the crack tip. (a), (b) and (c) are the schematic diagram, displacement contour plot and atomic structure respectively from EAM-QC calculation for K_I=0.198 eV/Å$^{2.5}$. (d)–(f) are the same from QCDFT calculation for K_I=0.169 eV/Å$^{2.5}$. (For interpretation of the references to color in this figure legend, the reader is referred to the web version of this article.)

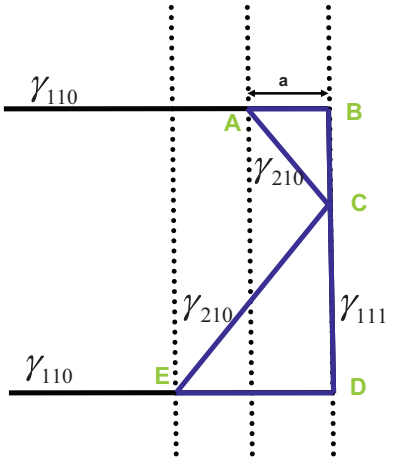

Fig. 9. A simple model for the crack tip profile. The dotted line represents the relevant slip planes near the crack tip. The rectangular line segments $\overline{AB}+\overline{BD}+\overline{DE}$ and the zigzag segments $\overline{AC}+\overline{CE}$ approximate EAM-QC and QCDFT crack tip profile respectively.

Table 1
Relevant quantities calculated by VASP and EAM for bulk Al; the corresponding experimental values are extrapolated to T=0 K.

	a_0 (Å)	γ_{111} (J/m^2)	γ_{110} (J/m^2)	γ_{210} (J/m^2)	γ_{sf} (J/m^2)	γ_{us} (J/m^2)	γ_{ut} (J/m^2)	τ_t
EAM	3.99	0.60	0.98	1.10	0.124	0.134	0.180	0.89
DFT	3.99	70.93	1.31	1.18	0.148	0.205	0.262	0.93
Exp	4.032	1.14[a]	1.14[a]	1.14[a]	0.12			

[a] Estimates for an "average" orientation.

segments $\overline{AC}+\overline{CE}$ are favored in QCDFT can be understood from the following surface energy analysis. Without loss of generality, we consider here the case where two dislocations are emitted for both EAM-QC and QCDFT. The length of $\overline{BC}$ equals to the magnitude of the Burgers vector because a full dislocation has been emitted upper-ward from A. As a result, $\overline{AC}$ represents a {2 1 0} surface. There are two layers of atoms removed in the initial crack opening, which is one Burgers vector wide. Therefore in addition to a full dislocation emitted downward from E, the length of $\overline{CD}$ equals to twice of the Burgers vector magnitude. Hence $\overline{CE}$ is also a {2 1 0} surface. Therefore $\overline{BD}$, $\overline{AC}$ (and $\overline{CE}$) and $\overline{AB}$ (and $\overline{ED}$) represents (1 1 1), {2 1 0} and ($\bar{1}$ 1 0) surface respectively. The total surface energy associated with the zigzag and rectangular segments can be written as $(\overline{AC}+\overline{CE})\gamma_{210}z_0$ and $(\overline{AB}\gamma_{110}+\overline{BD}\gamma_{111}+\overline{DE}\gamma_{110})z_0$, respectively. z_0 is the repeat distance along z-axis. The various surface energies have been calculated by both DFT and rescaled EAM as summarized in Table 1. For this particular crack configuration, the surface energy of the rectangular segments is 0.05 eV lower than that of the zigzag segments based on EAM energetics. On the other hand, the surface energy of the zigzag segments is 1.23 eV lower than that of the rectangular segments according to the DFT energetics.[2] Therefore, the zigzag segments are preferred in QCDFT while the rectangular segments are favored in EAM-QC. The same conclusion holds for other loadings as well.

5.2. Deformation twinning at the crack tip

According to the Peierls criterion of deformation twinning at a crack tip (Tadmor and Hai, 2003), one can define twinnability which is the likelihood of a material to twin as opposed to slip at the crack tip. The dimensionless twinnability can be expressed as (Tadmor and Bernstein, 2004)

$$\tau_t = \left[1.136 - 0.151\frac{\gamma_{\rm sf}}{\gamma_{\rm us}}\right]\sqrt{\frac{\gamma_{\rm us}}{\gamma_{\rm ut}}} \tag{4}$$

The coefficients 1.136 and 0.151 are universal constants for an fcc lattice. $\gamma_{\rm sf}$, $\gamma_{\rm us}$, and $\gamma_{\rm ut}$ are intrinsic stacking fault, unstable stacking fault and unstable twinning energy respectively. A material will emit a dislocation before twinning if $\tau_t < 1$ and will twin first if $\tau_t > 1$. Our DFT and EAM calculations find that τ_t is less than 1 as shown in Table 1, which

[2] $a=\sqrt{1/3}a_0$ where a_0 is the lattice constant. $\overline{AB}=a$, $\overline{BC}=\sqrt{3/2}a$, $\overline{BC}=\sqrt{6}a$, $\overline{DE}=2a$, $\overline{AC}=\sqrt{5/2}a$, $\overline{CE}=\sqrt{10}a$, and $z_0=\sqrt{9/2}a$. Taking a=2.3036 Å, the total surface energy of the zigzag configuration is 3.67 eV for EAM and 3.93 eV for DFT. The total surface energy of the rectangular segments is 3.62 eV for EAM and 5.16 eV for DFT.

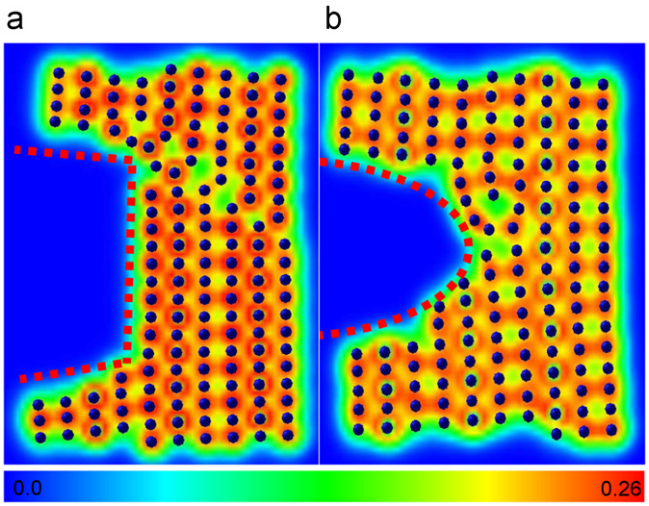

Fig. 10. The electron charge density ($Å^{-3}$) at the crack tip for (a) EAM-QC at K_I=0.198 eV/$Å^{2.5}$ and (b) QCDFT at K_I=0.169 eV/$Å^{2.5}$. The density contours range from 0 (blue) to 0.26 (red). The blue sphere stands for atomic position and the dashed line is an approximate profile of the charge density contours. (For interpretation of the references to color in this figure legend, the reader is referred to the web version of this article.)

suggests that no true deformation twinning along (1 1 1) plane be formed, consistent with the QCDFT and EAM-QC simulation results. However, a two-layer-wide micro-twin along (1 $\bar{3}$ $\bar{1}$) plane is formed in EAM-QC while no such twin is present in QCDFT. The distinction between the QCDFT and EAM-QC results is due to the large discrepancy of γ_{us}, which is the energy barrier for a leading partial nucleation at a crack tip (Rice, 1992). The large DFT value of γ_{us} renders the nucleation of the leading partial difficult, which in turn prohibits the formation of deformation twinning. We emphasize that the micro-twin is not a real twin, but a twin-like defect due to the shears at the crack tip.

5.3. Electron density at the crack tip

In Fig. 10, we present the electron charge density around the crack tip for the EAM-QC configuration of K_I=0.198 eV/$Å^{2.5}$ (left) and the QCDFT configuration of K_I=0.169 eV/$Å^{2.5}$ (right). The charge density for EAM-QC is determined by a superposition of atomic densities (obtained by VASP) centered at each EAM atoms. The distortion of charge density due to the defects is clearly visible. In EAM-QC the atomic bonding is weakened along the twin plane while in QCDFT the atomic bonding is significantly disrupted at the center of the crack. More importantly, the charge density profile of QCDFT is smoother than that of EAM-QC as indicated by the dashed curves. The "sharp" corners of EAM-QC charge density lead to higher kinetic energy of electrons. Since EAM-QC does not involve quantum mechanics, the "sharp corner" is not penalized energetically and thus permissible. Of course, the electron charge density profile reflects the underlying atomic structure: "sharp corners" correspond to a straight crack front thanks to a single active slip plane; smooth corners correspond to a more rounded crack front.

6. Conclusion

In summary, we have carried out a comparative study of fracture in Al by using two distinctive atomic interactions: quantum mechanical density functional theory and empirical embedded atom method. The DFT description of the crack tip is achieved by QCDFT method while the empirical description by EAM-QC method. In addition to quantitative differences, qualitatively different fracture behaviors are also observed between the two methods. EAM-QC predicts a more or less rectangular crack tip configuration while QCDFT yields a more rounded tip profile. The difference is due to the fact that the emitted dislocations glide on a single slip plane in EAM-QC while two adjacent slip planes are active in QCDFT. As the stress intensity factor is increased, more and more dislocations are emitted from the crack tip in EAM-QC while the number of dislocations remains the same up to the maximum loading applied in QCDFT calculations. A micro-twin is observed at the crack tip in EAM-QC, but it is absent in QCDFT. The electron density profile at the crack tip is also different between EAM-QC and QCDFT. All these differences can be understood in terms of defect energetics, including surface energy and stacking fault energy.

The different results received suggest that the atomic nature of crack tips is important and an accurate description of the atomic interaction at the crack tips is indispensable. Although empirical potentials can be developed by fitting to DFT results, it is unlikely that they will reproduce all *relevant* DFT energetics. This is particularly true since one does not know *a priori* what are the relevant energetics for a given crack. If several chemical species are present in a crack tip, the task of fitting a satisfactory potential becomes even more daunting. Therefore the solution lies at an explicit quantum mechanical

description of the crack tip, most likely in a form of DFT-based multiscale modeling, such as QCDFT. Of course, one should also be aware of the coupling errors in this type of multiscale approaches (Liu et al., 2007) and take the results with a grain of salt. The present paper concerns atomistic aspect of fracture which is important for many purposes. However, there are interesting fracture phenomena that do not depend on atomistic features and thus are beyond the scope of the present paper. Finally, we have not touched upon fracture dynamics. The questions—such as will finite temperature dynamics amplify or diminish the differences that we observed and what are the best strategies to implement dynamics in a multiscale setting—remain unanswered. We hope that the present paper could inspire more research effort in answering these questions.

Acknowledgments

We thank Ellad Tadmor for his assistance of constructing the crack model and many helpful discussions. The work at California State University Northridge was supported by the Office of Navel Research.

References

Bernstein, N., Hess, D.W., 2003. Lattice trapping barriers to brittle fracture. Phys. Rev. Lett. 91 (2), 025501.
Bernstein, N., Kermode, J.R., Csanyi, G., 2009. Hybrid atomistic simulation methods for materials systems. Rep. Prog. Phys. 72, 026501.
Broughton, J.Q., Abraham, F.F., Bernstein, N., Kaxiras, E., 1999. Concurrent coupling of length scales: methodology and application. Phys. Rev. B 60 (4), 2391.
Buehler, M.J., van Duin, A.C.T., Goddard III, W.A., 2006. Multiparadigm modeling of dynamical crack propagation in silicon using a reactive force field. Phys. Rev. Lett. 96 (9), 095505.
Choly, N., Lu, G.E.W., Kaxiras, E., 2005. Multiscale simulations in simple metals: a density-functional-based methodology. Phys. Rev. B 71 (9), 094101.
Csányi, G., Albaret, T., Payne, M.C., De Vita, A., 2004. Learn on the fly: a hybrid classical and quantum-mechanical molecular dynamics simulation. Phys. Rev. Lett. 93 (17), 175503.
Ercolessi, F., Adams, J.B., 1994. Interatomic potentials from 1st-principles calculations—the force-matching method. Europhys. Lett. 26 (8), 583.
Gavini, V., Bhattacharya, K., Ortiz, M., 2007. Quasi-continuum orbital-free density-functional theory: a route to multi-million atom non-periodic DFT calculation. J. Mech. Phys. Solids 55 (4), 697.
Griffith, A.A., 1920. The phenomenon of repture and flow in solids. Philos. Trans. R. Soc. London A 221, 163.
Hai, S., Tadmor, E.B., 2003. Deformation twinning at aluminum crack tips. Acta Mater. 51 (1), 117.
Hayes, R.L., Ho, G., Ortiz, M., Carter, E.A., 2006. Prediction of dislocation nucleation during nanoindentation of Al3Mg by the orbital-free density functional theory local quasicontinuum method. Philos. Mag. 86, 2343.
Hirth, J.P., Lothe, J., 1970. Theory of Dislocations. McGraw-Hill, New York.
Hoagland, R.G., Foiles, S.M., Baskes, M.I., Daw, M.S., 1990. An atomic model of crack tip deformation in aluminum using an embedded atom potential. J. Mater. Res. 5, 313.
Kohlhoff, S., Gumbsch, P., Fischmeister, H.F., 1991. Crack-propagation in bcc crystals studied with a combined finite-element and atomistic model. Philos. Mag. A 64, 851.
Kresse, G., Hafner, J., 1993. Ab initio molecular dynamics for liquid metals. Phys. Rev. B 47, 558.
Kresse, G., Furthuller, J., 1996a. Efficiency of ab-initio total energy calculations for metals and semiconductors using a plane-wave basis set. Comput. Mater. Sci. 6, 15.
Kresse, G., Furthuller, J., 1996b. Efficient iterative schemes for ab initio total-energy calculations using a plane-wave basis set. Phys. Rev. B 54, 11169.
Kresse, G., Hafner, J., 1994. Ab initio molecular-dynamics simulation of the liquid-metal–amorphous-semiconductor transition in germanium. Phys. Rev. B 49, 14251.
Liu, Y., Lu, G., Chen, Z., Kioussis, N., 2007. An improved QM/MM approach for metals. Simulation Mater. Sci. Eng. 15, 275.
Lu, G., Kaxiras, E., 2005. Overview of multical simulations of materials. In: Theoretical and Computational Nanotechnology. American Scientific Publisher, Stevenson Ranch, CA (Chapter 22).
Lu, G., Tadmor, E.B., Kaxiras, E., 2006. From electrons to finite elements: a concurrent multiscale approach for metals. Phys. Rev. B 73, 024108.
Miller, R., Tadmor, E.B., Phillips, R., Ortiz, M., 1998. Quasicontinuum simulation of fracture at the atomic scale. Modelling Simulation Mater. Sci. Eng. 6, 607.
Mills, M.J., Stadelmann, P., 1989. A study of the structure of lomer and 60-degrees dislocations in aluminum using high-resolution transmission electron-microscopy. Philos. Mag. A 60 (3), 355–384.
Monkhorst, H.J., Pack, J.D., 1976. Special points for Brillouin-zone integrations. Phys. Rev. B 13, 5188.
Ogata, S., Lidorikis, E., Shimojo, F., Nakano, A., Vashishta, P., Kalia, R.K., 2001. Hybrid finite element moleculardynamics electronic density functional approach to materials simulations on parallel computers. Comput. Phys. Commun. 138 (2), 143.
Peng, Q., Zhang, X., Hung, L., Carter, E.A., Lu, G., 2008. Quantum simulation of materials at micron scales and beyond. Phys. Rev. B 78, 054118.
Rice, J.R., 1992. Dislocation nucleation from a crack tip: an analysis based on the Peierls concept. J. Mech. Phys. Solids 40, 239.
Shenoy, V.B., Miller, R., Tadmor, E.B., Rodney, D., Phillips, R., Ortiz, M., 1999. An adaptive finite element approach to atomic-scale mechanics—the quasicontinuum method. J. Mech. Phys. Solids 47, 611.
Sih, G.C., Liebowitz, H., 1968. Mathematical theories of brittle fracture, In: Fracture: An Advanced Treatise, vol. 2. Academic, New York, p. 68.
Tadmor, E.B., Bernstein, N., 2004. A first-principles measure for the twinnability of FCC metals. J. Mech. Phys. Solids 52, 2507.
Tadmor, E.B., Hai, S., 2003. A Peierls criterion for the onset of deformation twinning at a crack tip. J. Mech. Phys. Solids 51, 765.
Tadmor, E.B., Miller, R., Phillips, R., 1999. Nanoindentation and incipient plasticity. J. Mater. Res. 14, 2249.
Tadmor, E.B., Miller, R.E., 2005. The theory and implementation of the quasicontinuum method. In: Handbook of Materials Modeling, vol. 1. Kluwer Academic Publishers.
Van der Giessen, E., Needleman, A., 2002. Micromechanics simulations of fracture. Ann. Rev. Mater. Res. 32, 141.
Zhang, X., Lu, G., 2007. Quantum mechanics/molecular mechanics methodology for metals based on orbital-free density functional theory. Phys. Rev. B 76, 245111.